Inhibitor-Induced Conformational Change in Cytochrome P-450$_{CAM}$[†,‡]

Reetta Raag,[§,∥] Huiying Li,[§,⊥] B. C. Jones,[▽] and Thomas L. Poulos*[,§,⊥]

Center for Advanced Research in Biotechnology of the Maryland Biotechnology Institute, University of Maryland at Shady Grove, 9600 Gudelsky Drive, Rockville, Maryland 20850, and Department of Drug Metabolism, Pfizer Central Research, Sandwich, Kent, England

Received November 12, 1992; Revised Manuscript Received February 8, 1993

ABSTRACT: The X-ray crystal structures of cytochrome P-450$_{CAM}$ complexed with both enantiomers of a chiral, multifunctional inhibitor have been refined to R-factors of 21.0% [(+)-enantiomer] and 19.6% [(−)-enantiomer] at approximately 2.1-Å resolution. Binding of either enantiomer, both considerably larger than the natural substrate camphor, results in similar, dramatic structural changes in the enzyme. In contrast to all previous P-450$_{CAM}$ crystallographic structures, the Tyr96 side chain is not pointing "down" toward the heme but is rather directed "up" into the proposed substrate access channel. This conformational change is accompanied by the displacement of the Phe193 side chain out into the solvent at the enzyme surface. These changes are consistent with the assignment of this region of the enzyme as the access channel [Poulos et al. (1986) *Biochemistry 25*, 5314–5322] and suggest that several aromatic residues lining the channel may be involved in substrate recognition and channeling to the active site. The cation usually observed coordinated to the Tyr96 carbonyl oxygen is missing in the presence of the (+)-enantiomer but is present with the (−)-enantiomer. The Phe87 side chain, located near the inhibitor binding site, adopts different orientations depending upon which enantiomer is bound. Finally, electron density reveals that although the inhibitor enantiomers were dichlorinated as provided, when bound to P-450$_{CAM}$ the chlorine atoms are present at only 0–20% occupancy, probably reflecting selective binding of impurities in the samples. Coordinates of these inhibited P-450$_{CAM}$ complexes have been deposited in the Brookhaven Protein Data Bank [Bernstein et al. (1977) *J. Mol. Biol. 112*, 535–542].

Cytochrome P-450$_{CAM}$ is a member of the P-450 superfamily of enzymes which are involved in a multitude of biochemical processes and which metabolize a seemingly endless array of relatively hydrophobic organic substrates, physiological as well as exogenous. P-450 enzymes participate in steroid hormone and bile acid biosynthesis, vitamin activation, fatty acid hydroxylation, and detoxification of foreign compounds including solvents, antibiotics, anesthetics, insecticides, and polycyclic aromatic hydrocarbons (Nebert et al., 1981; Nebert & Gonzalez, 1987; Anders, 1985). Unfortunately, their detoxification activity is occasionally also associated with the carcinogenic activation of exogenous compounds. A better structural understanding of P-450 enzymes should facilitate inhibitor design for deleterious P-450 isozymes as well as the engineering of novel P-450-like enzymes to metabolize organic compounds which are environmentally undesirable.

P-450$_{CAM}$ is a bacterial camphor hydroxylase which has been extensively studied biochemically (Gunsalus et al., 1974; Debrunner et al., 1978; Gunsalus & Sligar, 1978; Ullrich, 1979; Wagner & Gunsalus, 1982). X-ray crystal structures have been determined of the camphor-free and -bound forms of this enzyme (Poulos et al., 1985, 1986, 1987), of the enzyme complexed with various alternate substrates (Raag & Poulos, 1989a, 1991, 1992) and inhibitors (Poulos & Howard, 1987; Raag & Poulos, 1989b; Raag et al., 1990), and of the Thr252Ala mutant enzyme in which electron transfer is uncoupled from camphor hydroxylation (Raag et al., 1991). However, a mystery of some duration is how P-450$_{CAM}$ substrates actually enter the enzyme, since once in the active site, all substrates and inhibitors investigated have proved to be essentially completely buried from solvent exposure. Here we describe two structures of P-450$_{CAM}$ in which the enzyme is complexed individually with both enantiomers of an inhibitor consisting of a chiral center with imidazolylmethyl, dichlorophenyl, hexyl, and hydroxyl substituents (Figure 1; Richardson et al., 1990). More than twice the size of the natural substrate camphor, this inhibitor causes dramatic structural changes in the enzyme upon binding. These changes are consistent with the proposed location of the access channel—a suggestion made following the determination of the substrate-free P450$_{CAM}$ structure (Poulos et al., 1986), which revealed several regions of enhanced thermal mobility with respect to the camphor-bound structure.

MATERIALS AND METHODS

Recombinant P-450$_{CAM}$ was purified and crystallized according to published procedures (Poulos et al., 1982; Unger et al., 1986; Atkins & Sligar, 1988). Substrate-free crystals were initially soaked in an enantiomeric mixture of the inhibitor (Pfizer compound UK-39671), provided by Pfizer Central Research, Sandwich, Kent, England. This compound had been synthesized at Pfizer as part of a search for novel antifungal agents (Richardson et al., 1990) but had also been found to be an inhibitor of the bacterial enzyme cytochrome P-450$_{CAM}$. However, following even an overnight soak in the enantiomeric mixture, crystals of P-450$_{CAM}$ were either cracked or yielded diffraction data of poor quality. Subsequently, Pfizer Central Research provided 10 mg of the monooxalate salt of each individual inhibitor enantiomer, UK-67254-13(+) and UK-67255-13(−). Both structures described

† Supported in part by NIH Grant GM 33688.

‡ Coordinates have been deposited with the Brookhaven Protein Data Bank. Assigned codes are 1PHA [(+)-enantiomer] and 1PHB [(−)-enantiomer].

* To whom correspondence should be addressed.

§ University of Maryland at Shady Grove.

∥ Present address: Enzon, Inc., 16020 Industrial Dr., Gaithersburg, MD 20877.

⊥ Present address: Department of Molecular Biology and Biochemistry, University of California, Irvine, CA 92717.

▽ Pfizer Central Research.

0006-2960/93/0432-4571$04.00/0

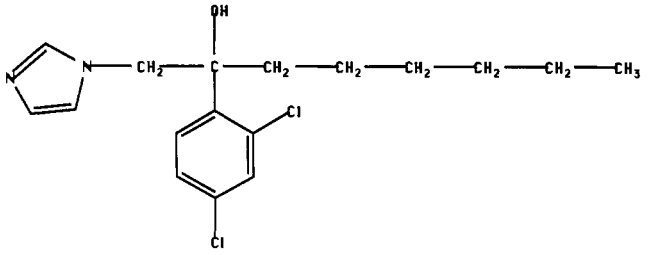

FIGURE 1: Structure of inhibitor.

Table I: Data Collection Summary

inhibitor enantiomer:	(+)	(−)
maximum resolution (Å)	2.11	2.06
total observations	90 005	75 552
R_{sym}[a]	0.061	0.067
% data collected to	3.83 Å 99	3.74 Å 100
	3.04 Å 100	2.97 Å 100
	2.65 Å 100	2.59 Å 100
	2.41 Å 100	2.36 Å 97
	2.24 Å 99	2.19 Å 93
	2.11 Å 82	2.06 Å 80
$I/\sigma(I)$	2.41 Å 2.55	2.36 Å 2.22
	2.24 Å 1.75	2.19 Å 1.49
	2.11 Å 1.39	2.06 Å 0.85

[a] $R_{sym} = \Sigma|I_i - \langle I_i\rangle|/\Sigma I_i$ = intensity of the ith observation and $\langle I_i\rangle$ = mean intensity.

here were determined for the individual enantiomers bound to P-450$_{CAM}$. A schematic structure of the inhibitor is shown in Figure 1.

Substrate-free crystals were soaked overnight in a mother liquor consisting of 40% saturated ammonium sulfate, 0.05 M potassium phosphate, and 0.25 M KCl at pH 7.0, with inhibitor enantiomer concentrations of about 10–20 mM. Higher inhibitor concentrations resulted in the appearance of cracks in the crystals. X-ray diffraction data were collected from single crystals of inhibitor-bound P-450$_{CAM}$ using a Siemens area detector/Rigaku rotating anode and processed using the XENGEN program package (Howard et al., 1987). Greater than 90% of diffraction data were collected to 2.2 Å for both enantiomeric complexes and R_{sym} was 0.061 and 0.067 for (+) and (−) enantiomeric complexes, respectively. Other data collection statistics are presented in Table I.

Crystallographic refinement was carried out using the restrained parameters–least-squares package of programs of Hendrickson and Konnert (1980) and is summarized in Table II. Initial $F_o - F_c$[1] and $2F_o - F_c$ difference Fourier maps were calculated using coordinates based on the 1.7-Å refined wild-type camphor-bound P-450$_{CAM}$ structure (Poulos et al., 1987), with camphor coordinates omitted, and with diffraction data [10-Å diffraction limit and with $F \geq 2\sigma(F)$] obtained from the crystalline complexes. $F_o - F_c$ maps were contoured at $\pm 3\sigma$ and $2F_o - F_c$ maps were contoured at +0.5 and $+1\sigma$ (σ is the standard deviation of the electron density map). The initial $F_o - F_c$ map for the (−)-enantiomer is shown in Figure 2. Similar large changes were observed in the side-chain positions of residues Tyr96 and Phe193 of the enzyme complexes with both inhibitor enantiomers, with respect to the camphor-bound structure. Thus, maps were also calculated with these and adjoining residues omitted from the phase calculation to remove model bias from the electron density. Inhibitor models were built and energy-minimized with QUANTA (Polygen), using a Silicon Graphics IRIS. Inhibitor models were fit to electron density maps, and the protein model was adjusted, using the molecular modeling package FRODO (Jones, 1978) operating on an Evans & Sutherland graphics station. The absolute configurations of the enantiomers provided were not known (until after the structures reported here had been modeled and refined), which led to considerable difficulty in electron density map interpretation (see below).

[1] Abbreviations: F_c, calculated structure factors; F_o, observed structure factors; R-factor, $\Sigma|F_o - F_c|/\Sigma F_o$; rms, root mean square.

Table II: Crystallographic Refinement Summary

inhibitor enantiomer:	(+)	(−)
resolution range (Å)	10.0–2.1	10.0–2.1
reflections measured	22 564	23 386
reflections used[a]	19 409	19 152
R-factor[b]	0.210	0.196
rms deviation of bond distances (Å)	0.020	0.018
bond angles (Å)	0.028	0.030
dihedral angles (Å)	0.030	0.036
non-hydrogen atoms	3482	3505
solvent molecules	205	213
discretely disordered residues[c]	M191, T192	M191, T192, R365, I395

[a] Reflections with $F > 2\sigma(F)$. [b] $R = \Sigma|F_o - F_c|/\Sigma F_o$. [c] Disorder of residues 191–192 and 395 appears to be related to inhibitor binding. R365 is a surface residue, disorder in which may or may not be significant.

Structures were judged to have refined sufficiently once $F_o - F_c$ maps showed little or no interpretable density when contoured at $\pm 3\sigma$. To provide an unbiased check on the fit of the models to electron density maps, final maps for both enantiomeric complexes were calculated omitting coordinates of the inhibitors, of active-site solvent, and of Phe87, Tyr96, and residues 191–193 from the phase calculations (Figure 3). Refined models were subjected to additional refinement without bond, angle, or nonbonded contact distance restraints to better estimate active-site distances. Final coordinates of P-450$_{CAM}$ complexed with the (+)-enantiomer are shown superimposed on those of the camphor-bound enzyme in Figure 4, and Figure 5 is a comparison of the two enantiomeric complexes. Temperature factor differences between refined inhibited structures and camphor-bound P-450$_{CAM}$ were computed as previously described (Poulos & Howard, 1987) and are shown in Figure 6.

Electron density maps showed minimum residual $F_o - F_c$ difference density with inhibitor chlorine occupancies in the range of 0–20%, and thus inhibitors were modeled with 20% chlorine occupancy and full occupancy for all other atoms. Since this model was inconsistent with the expected results (full occupancy for all atoms), remaining inhibitor samples were returned to Pfizer for mass spectral analysis, the results of which indicated the presence of minor monochloro and other impurities. The racemic mixture was found to contain even a dichloro impurity distinct from either enantiomer, which may have contributed to the destruction of crystals soaked in this sample.

RESULTS

Initial maps (Figure 2) indicated quite clearly that major structural changes had occurred in the enzyme upon binding of either enantiomer of the inhibitor. Surprisingly, these were almost entirely confined to dramatic reorientations of the Tyr96 and Phe193 side chains. The Tyr96 side chain, which points "down" toward the substrate and heme in all other structures we have determined, is directed "up" into the proposed access channel region in the presence of both inhibitor enantiomers. This structural rearrangement places the Tyr96 side chain approximately in the position occupied by the Phe193 side chain in the camphor-bound enzyme (Figure 4)

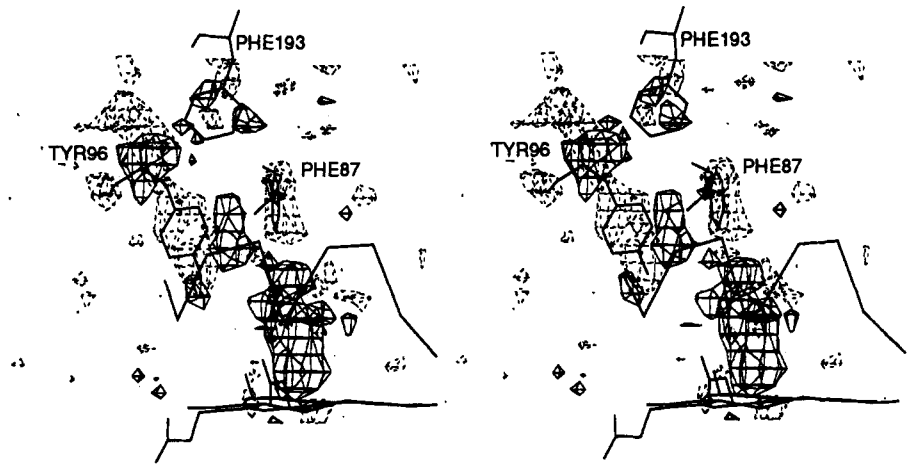

FIGURE 2: Stereoimage of the initial $F_o - F_c$ difference electron density map for the (–)-enantiomer-inhibited complex of P-450$_{CAM}$. Maps were calculated with diffraction amplitudes from a crystal of the inhibitor-bound protein and phases from camphor-bound P-450$_{CAM}$ (Poulos et al., 1987), omitting camphor coordinates but including residues Phe87, Tyr96, and Phe193. Map contours are at $\pm 3\sigma$ with negative and positive density depicted as dashed and solid lines, respectively. The active-site distal helix backbone and heme are shown, together with side chains which have undergone large, concerted structural rearrangements as a result of inhibitor binding. Note especially that side chains of residues Tyr96 and Phe87 are surrounded by negative (dashed) density, indicating they are no longer in their camphor-bound positions upon inhibitor binding. The density surrounding the Phe193 side chain is less interpretable in this initial map, since the (similar) side chain of Tyr96 has displaced it (i.e., there is not as dramatic a change in atomic occupancies at this location in space, in contrast to Tyr96 and Phe87, which move but are not replaced by similar chemical groups). Phe193 in turn is displaced into the solvent at the protein surface (density not shown in this view). Maps for the (+)-enantiomer are similar to those shown. Electron density representing the inhibitor is directly above the heme iron.

and presumably accounts for the displacement of the Phe193 side chain to the enzyme surface. The inhibitor is so large in comparison with the natural substrate camphor (22 vs 10 non-hydrogen atoms) that it is unlikely it could bind at all without such a drastic enlargement of the active site.

Maximum atomic displacements of the Tyr96 and Phe193 side chains are similar: 8.7 and 8.8 Å for the Tyr96 OH atom and 8.5 and 8.2 Å for the terminal C_z atom of the Phe193 ring [for (+)- and (–)-enantiomers, respectively]. The Phe193 side-chain motion is relatively simple and consists essentially of a 140° rotation, about the C_α–C_β bond direction, of Cγ and atoms terminal to it (i.e., the phenyl ring). Such a rotation, with minimal adjustments of other side-chain torsional angles, maps the Phe193 side chain of the camphor-bound enzyme to the position of the inhibited complexes. The Tyr96 side-chain motion is somewhat more complex and consists roughly of 80°, 180°, and –50° rotations of the side-chain C_β (and more distal atoms), the side-chain Cγ (and more distal atoms), and the hydroxyphenyl ring itself, again with respect to the camphor-bound enzyme.

Despite the large inhibitor-induced side-chain motions, the backbone of the protein remains essentially unchanged with respect to the camphor-bound structure. The only notable exception is the appearance of a second conformation, with the carbonyl oxygen directed about 180° away, for the 191–192 peptide group. Although it is possible to model the Tyr96/Phe193 conformational change using only correlated torsional rotations of these side chains, and without clashes with other protein groups, it is not at all clear whether this process actually occurs without accompanying backbone motion. We are hoping to address this question with molecular dynamics simulations in the future.

In contrast to the very interpretable protein density, the inhibitor density of both complexes was more ambiguous. The difficulty of inhibitor density interpretation was compounded by the fact that the absolute configurations of the two enantiomers were not initially known to us. Thus, we attempted to fit models of both enantiomers into maps of both crystalline complexes. However, once this paper had been submitted for review, Pfizer informed us of the absolute stereochemistries of the inhibitor enantiomers, and these are consistent with the assignments we had made on the basis of model-building, as described below.

A major obstacle in modeling these enantiomers was that neither map had continuous density for the entire aliphatic chain of the inhibitor (see Figure 3), rendering nearly impossible the location of this group with complete confidence. A further difficulty was that disorder was clearly apparent in both electron density maps. There is not a hand-in-glove fit between P-450$_{CAM}$ and these inhibitors, in contrast to the snug fit between camphor and the enzyme (Poulos et al., 1985). With the movement of the Tyr96 side chain, there is very little else hydrophilic in the active-site pocket to provide a hydrogen bond which would possibly stabilize a single inhibitor orientation. Although it is clear that the imidazole group is linked to the heme iron in both enantiomers, various different torsional orientations of the hydroxyl, dichlorophenyl, and aliphatic substituents about the chiral carbon may be present in these complexes. An assemblage of such configurational enantiomers destroys the clarity of the resulting electron density map, which is an average of all molecular complexes in the crystal lattice.

The inhibitor density for both enantiomers is very similar (see Figures 2 and 3). One explanation for this could be that P-450$_{CAM}$ is selectively binding a similar molecular species in both samples, which were found to contain some impurities. However, there are some arguments against this possibility: (1) Differences in temperature factors exist between the refined structures. (2) Fitting of the (+)-enantiomer model to the putative (–)-enantiomer maps leads to a clash between Phe98 and the tip of the aliphatic tail of the inhibitor, since there is electron density in the (–)-enantiomer map leading away from the direction taken by the aliphatic tail in the (+)-enantiomer map. (3) Differences between the two complexes in residues251–252, in the orientation of the Phe87 ring, and in solvent near residues Phe87 and Tyr96 also suggest they are distinct.

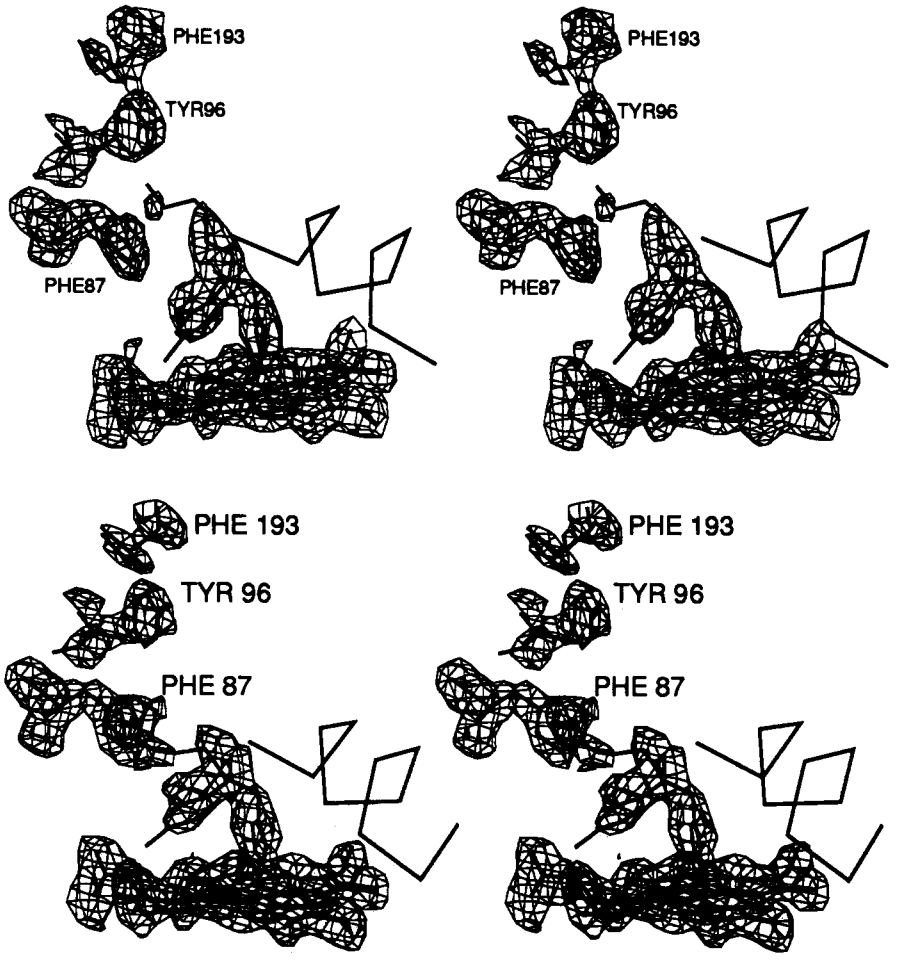

FIGURE 3: Stereoimages of the final $2F_o - F_c$ electron density maps of (top) (+)-enantiomer-inhibited and (bottom) (–)-enantiomer-inhibited P-450$_{CAM}$, each contoured at 1σ. Inhibitor coordinates, as well as those of residues Phe87, Tyr96, and Phe193, were omitted from the phase calculation to eliminate model bias. The backbone of the distal helix is shown to the right of the figure, as a reference. The heme is at the bottom of the figure. Electron density is similar for both enantiomeric complexes, except that the aliphatic tails of the two enantiomers, for both of which electron density is discontinuous, appear to pack on different sides of the Phe87 ring. Such broken density is consistent with high mobility and/or multiple inhibitor binding orientations. No electron density is observed for the inhibitor *o*-Cl atom, and the *p*-Cl atom is estimated to be present at less than 20% occupancy in both enantiomeric complexes. Connected density between Phe193 and Tyr96 and the poor quality of the Phe193 side-chain electron density, especially in the (+)-enantiomeric complex (top), suggest that the Phe193 side chain is not in a well-defined location at the hydrophilic surface of the enzyme and that Phe193 and Tyr96 side chains may occupy two different conformations, possibly reflecting incomplete inhibitor occupancy. However, only a single protein conformation has been modeled. We believe the figures shown represent the major enantiomer binding orientations, even in the absence of distinctive chlorine density, since the electron density in which the inhibitor dichlorobenzene ring has been modeled in both structures is flattened and pancakelike and provides a good fit for the 6-carbon portion of the ring. Conversely, the density in which the inhibitor hydroxyl and aliphatic groups have been modeled is more cylindrical and less conducive to the fit of a six-membered ring. Moreover, fitting of either enantiomer aliphatic tail to the density in which the dichlorobenzene constituent is shown leads to unresolvable clashes with other active-site groups not shown in these views.

After numerous attempts to fit the electron density of both inhibitor–enzyme complexes with atomic models of both enantiomers, considering all possible torsional configurations consistent with the maps, we are relatively confident of the *major* binding conformation of each enantiomer. Again, it is highly likely that multiple binding conformations of each inhibitor enantiomer are possible and present, and this in itself would account for the similarity in electron density for the two enantiomers. This scenario is probable for a compound with such great torsional flexibility, bound in a predominantly hydrophobic active site with few enzymatic groups offering definitive orientational direction. Unfortunately, the resulting electron density maps representing average conformations make modeling difficult, and we have not attempted to define more than a single probable conformation for each enantiomer.

The average atomic temperature factors for all protein and heme atoms are 19 Å^2 for camphor-bound P-450$_{CAM}$ (Poulos et al., 1987) and 19 and 20 Å^2 for the (+)- and (–)-enantiomeric inhibitor complexes, respectively. However, the inhibitor complexes have rms temperature factors 3.2 Å^2 (+) and 3.6 Å^2 (–) higher than the camphor-bound structure. For comparison, substrate-free P-450$_{CAM}$ (Poulos et al., 1986), with a solvent cluster in the active site, has an average atomic temperature factor of 22 Å^2 and an rms temperature factor 5.2 Å^2 higher than that of camphor-bound P-450$_{CAM}$. The average atomic temperature factors of the enzyme-bound inhibitor enantiomers themselves are 20 Å^2 (+) and 27 Å^2 (–), in contrast to 16 Å^2 for enzyme-bound camphor. As might be anticipated from these values, residues structurally disturbed by inhibitor binding all show large fluctuations in mobility with respect to the camphor-bound enzyme. Specifically, average atomic temperature factors for side-chain atoms of residues Phe87, Tyr96, and Phe193 respectively are 11, 13, and 21 Å^2 in the presence of camphor (Poulos et al., 1987), 14, 17, and 30 Å^2 in the presence of the (+)-enantiomer, and 20, 34, and 40 Å^2 in the presence of the (–)-enantiomer.

In both inhibited structures, the regions surrounding residues Tyr96 and Phe193 are also considerably more mobile, by up

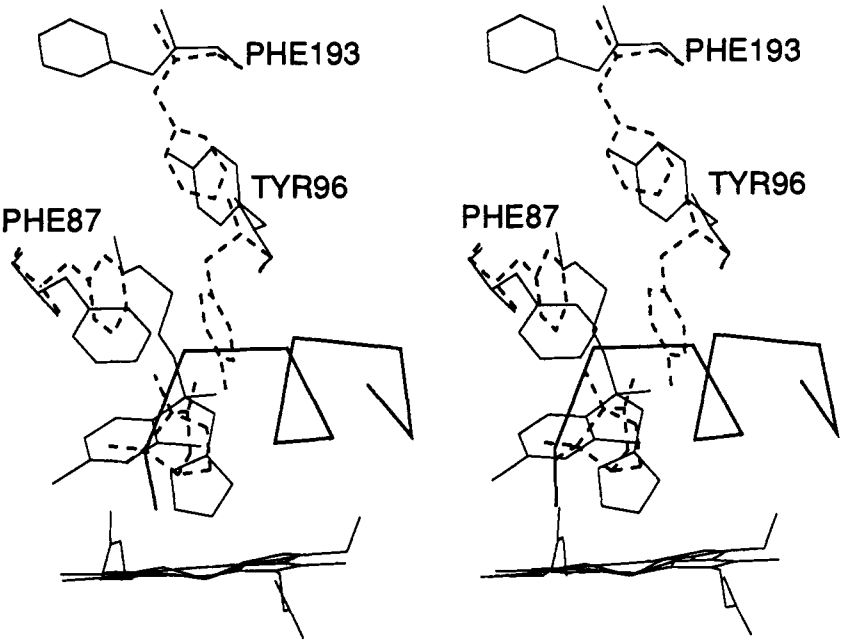

FIGURE 4: Structural comparison of (+)-enantiomer-inhibited (solid lines) and camphor-bound (dashed lines) P-450$_{CAM}$ complexes. The distal helix backbone is again shown for reference. Despite dramatic side-chain rearrangements, the protein backbone and heme are essentially unchanged by inhibitor binding. Note the inhibitor-induced reorientation of the Phe87 ring and upward displacements of Tyr96 and Phe193 side chains with respect to the camphor-bound enzyme.

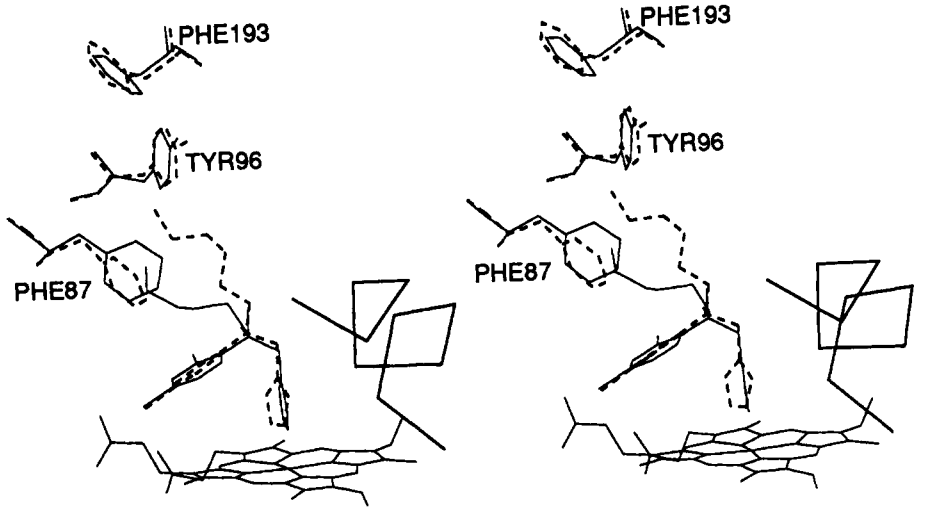

FIGURE 5: Structural comparison of (−)-enantiomer-inhibited (solid lines) and (+)-enantiomer-inhibited (dashed lines) P-450$_{CAM}$ complexes, with distal helix backbone and heme. Note enantiomer-dependent differences in inhibitor aliphatic tail packing against the Phe87 side chain.

to about 15–20 Å^2 [(−)-enantiomer], than in camphor-bound P-450$_{CAM}$ (Figure 6a,b). Residues near 80–100 are more mobile in the presence of the (−)-enantiomer, and residues in the general region 190–230 are slightly more mobile with the (+)-enantiomer (Figure 6c), possibly due to packing differences between protein and different enantiomers.

DISCUSSION

The camphor-bound P-450$_{CAM}$ structure (Poulos et al., 1985, 1987) showed that Tyr96 is located in the active site of the enzyme but also at the end of a narrow channel connecting this deeply-buried feature with the molecular surface. The substrate-free P-450$_{CAM}$ structure (Poulos et al., 1986) furthermore revealed that temperature factors of residues contained in several loops which form this channel are considerably higher, suggesting greater atomic motion, in the absence of camphor. This finding as well as lack of any other obvious route suggested that this loop region is the substrate access channel. The large changes in residues Tyr96 and Phe193 in the inhibited structures of cytochrome P-450$_{CAM}$ reported here are consistent with this hypothesis.

However, in no P-450$_{CAM}$ structure determined to date, including the enzyme–inhibitor complexes reported here, is the channel of sufficient diameter to permit a molecule the size of camphor to travel through it. This is the case even when side chains of the channel-lining residues are stripped off for a van der Waals surface calculation of the protein backbone around the channel. Thus, these new structures do not definitively prove the location of the access channel. They do indicate, however, that if Tyr96 and Phe193 are located along the channel, even more motion than has been observed in these structures must take place for substrate entry and product exit. There is some hint of this from the higher temperature factors of inhibited versus camphor-bound P-450$_{CAM}$ (see below and Figure 6). Moreover, the quality of the electron density in the channel-lining loop regions is generally poorer than that in substrate complexes we have determined.

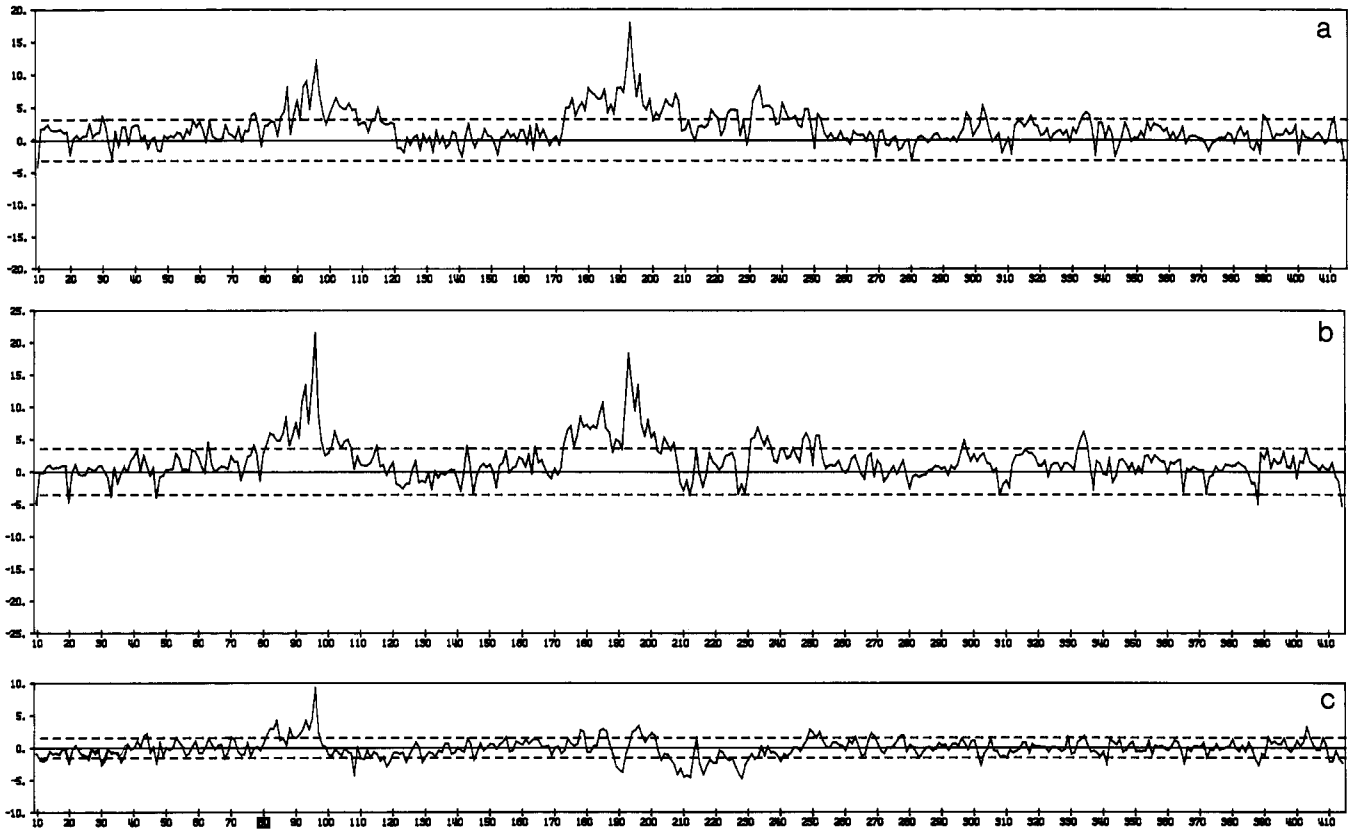

FIGURE 6: Mean temperature factor differences between inhibited and camphor-bound P-450$_{CAM}$. Residue number is plotted along the abscissa and ΔB (square angstroms) along the ordinate. Dashed lines indicate the root mean square difference in mean temperature factors. (a, top) (+)-Enantiomer – camphor (rms Δ = 3.2 Å^2). (b, middle) (–)-Enantiomer – camphor (rms Δ = 3.6 Å^2). (c, bottom) (–)-Enantiomer – (+)enantiomer (rms Δ = 1.6 Å^2).

Some minor differences exist between the two enantiomeric structures reported here: (1) The cation which coordinates to the carbonyl oxygen of Tyr96 is present with the (–)-enantiomer but not with the (+)-enantiomer. (2) The solvent structure in the active site and channel regions is somewhat different in the two complexes. There is a solvent molecule between the side-chain hydroxyl group of Tyr96 and the Phe193 carbonyl oxygen, in the presence of the (–)-enantiomer only. However, the geometry between these groups does not suggest a very strong hydrogen bond, and Tyr96 is actually more mobile with the (–)-enantiomer. (3) There is some indication of a minor conformation with the Tyr96 and Phe193 side chains "down" in the presence of the (+)-enantiomer. This may account for the slightly higher *R*-factor of this complex but does not explain why Tyr96 temperature factors are higher with the (–)-enantiomer. However, we have only modeled a single protein conformation for both enantiomeric complexes reported here. (4) The orientation of the Phe87 ring differs by approximately 90° in the two enantiomeric complexes, which can be accounted for by the enantiomer-dependent packing of the aliphatic substituent against this side chain. (5) The O_2-binding groove region of the distal helix is essentially identical in camphor-bound and (+)-enantiomer-inhibited P-450$_{CAM}$. In contrast, with the (–)-enantiomer, the Thr252 side chain is farther from Gly248, and the Asp251 carbonyl oxygen is directed along the helix axis. These changes resemble those observed in the Thr252Ala mutant enzyme (Raag et al., 1991) and may be due to enantiomeric packing differences in the active site. (6) Finally, a second conformation of the active-site residue Ile395 has been observed and modeled in the presence of the (–)-enantiomer. The significance of this second conformation is currently unclear.

Plots of the difference in mean temperature factor between inhibited and camphor-bound P-450$_{CAM}$ (Figure 6a,b) are extremely reminiscent of similar plots for the substrate-free minus camphor-bound enzyme (Poulos et al., 1986). With respect to the camphor-bound enzyme, peaks nearly 20 Å^2 higher occur in the inhibited complexes, centered around residues Tyr96 and Phe193. It is interesting that, in the camphor-bound structure, the backbone atoms of Tyr96 are more mobile (17 Å^2 average) than those of the side chain (13 Å^2 average), presumably due to the hydrogen bond between the Tyr96 side chain and camphor in the active site. In the absence of this interaction, the Tyr96 side chain can be extremely mobile. This observation, as well as previous indications of second, minor Tyr96/Phe193 conformations [unpublished data on 11-week adamantane structures discussed in Raag et al. (1991)], prompted a reevaluation of the substrate-free P-450$_{CAM}$ diffraction data (see Figure 7). It was very exciting to observe that these data can be modeled somewhat better by assuming a second conformation in which both Tyr96 and Phe193 side chains are "up" in the substrate-free enzyme as well (unpublished work).

The potential existence of a Tyr96/Phe193 "up" conformer in the substrate-free enzyme suggests a possible function for Phe193 and perhaps for other aromatic or hydrophobic residues (Tyr29, Phe98, Ile395) lining the still-putative access channel, shown in Figure 8. Protein surfaces are generally coated with hydrophilic and charged groups. However, the substrates of P-450 enzymes tend to be hydrophobic compounds. In the substrate-free enzyme, an aromatic residue with high mobility and a partial surface conformation such as Phe193 may function as a solvent-accessible hydrophobic patch that aids in guiding substrates to the active site. Phe193 could also temporarily block substrate escape from the active site by

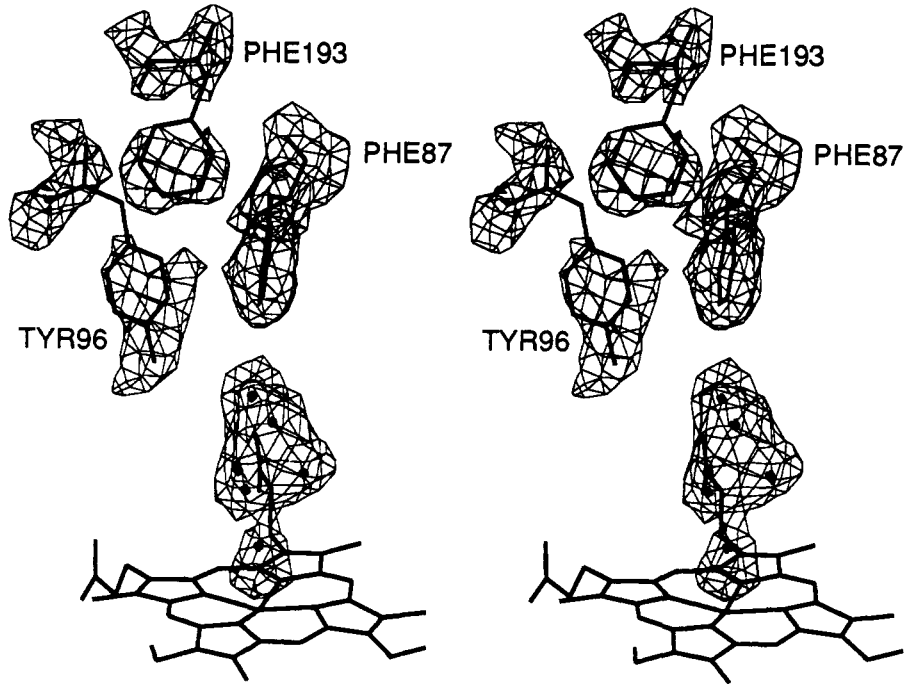

FIGURE 7: Final $2F_o - F_c$ map, contoured at 1σ, of substrate-free P-450$_{CAM}$ (Poulos et al., 1986). The active site includes a cluster of solvent molecules, one ligated distally to the heme iron atom. Note that whereas electron density for most active-site residues is well-defined (Phe87 is shown as an example), electron density is not continuous between the side chains and backbones of residues Tyr96 and Phe193. This suggests that, in the substrate-free enzyme, an alternate conformation may exist in which the Tyr96 side chain displaces that of Phe193 to the enzymatic surface, similar to that seen in the inhibited complexes reported here.

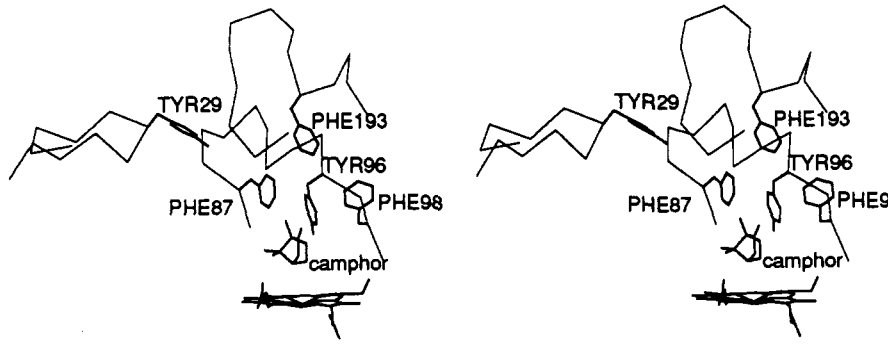

FIGURE 8: Backbones of loops and aromatic side chains defining putative access channel region in P-450$_{CAM}$. Coordinates shown are those of the camphor-bound complex (Poulos et al., 1987). Aromatic residues may play a role in channeling hydrophobic substrates and products into and out of the enzyme.

swinging to its "down" conformation in association with substrate entry into the channel. These hypotheses could be addressed with site-directed mutagenesis and molecular dynamics experiments.

Finally, the question remains as to why the inhibitor chlorine occupancy is only partial in these structures. It may be of significance that the enzyme active site does not appear large enough to accommodate a dichlorinated inhibitor. Since minor monochloro impurities have been identified in the inhibitor samples, it is feasible that steric constraints may have selected for the binding of partially dechlorinated species.

However, the possibility does exist that halide elimination or substitution has occurred [for extensive reviews see Màzor (1975) and Patai and Rappoport (1983)]. Reductive photodehalogenation is known to be especially facile in the presence of electron-rich compounds such as water and aromatic groups, both of which are found in the P-450$_{CAM}$ active site. X-rays may perhaps have induced electron transfer from the nearby Phe87 ring to the inhibitor, promoting halogen departure. Depending on solvent conditions, halogen elimination may occur primarily by nucleophilic, electrophilic, or radical mechanisms, or different mechanisms may compete. Generally, nonpolar conditions favor homolysis of the carbon–halogen bond, whereas increased solvent polarity promotes heterolysis.

Ionizing radiation decomposes water to form hydroxyl radicals which may add to unsaturated aliphatic or aromatic compounds, abstract hydrogen radicals or electrons, or react with another radical to form a stable product (Dorfman & Adams, 1973). Thus nucleophilic displacement of chlorine by solvent-derived hydroxyl may compete with halogen elimination from the inhibitor. However, the electron density is still only consistent with partial occupancy of even hydroxyl substituents of the inhibitor benzene ring. Yet another possibility is derivatization of the Phe87 side chain by a hydroxyl or chlorine radical. The electron density of this phenyl ring is somewhat extended at the meta position, which could be consistent with some kind of chemical transformation. Another dechlorination possibility is suggested by Figure 5. The refined model of the (−)-enantiomer is rather strained geometrically, with the *o*-chlorine quite close to the hexyl substituent. However, this configuration fits the electron density, which may include a contribution from an internally cyclized inhibitor configuration. Such a species could result

if a departing *o*-chlorine radical abstracted a hydrogen radical from the inhibitor aliphatic group, followed by intramolecular recombination of the hexyl and dechlorinated phenyl radicals.

CONCLUSIONS

Despite some lingering uncertainty regarding the exact chemical natures and orientaions of the inhibitor enantiomers bound in these complexes, one feature of both structures is irrefutable. Major structural changes, not comparable in magnitude to those observed in any previous P-450$_{CAM}$ complex, have been observed in residues Tyr96 and Phe193.

Modeling suggests that the conformational switch in Tyr96 and Phe193 side chains may be possible without any other attendant structural changes and without van der Waals clashes with the rest of the protein. However, in all P-450$_{CAM}$ structures determined to this point, including the inhibited complexes described here, the putative access channel is too narrow to permit the transit of a substrate-sized molecule. Therefore, complex protein deformations must mediate the transient opening of the channel, although unfortunately we have not yet observed such intermediates crystallographically.

ACKNOWLEDGMENT

We are grateful to Andy Howard and Marc Whitlow for making possible data collection at Enzon, Inc. (formerly Genex Corp.), Xinhua Ji for advice regarding figures, Jonathan Dill for figure generation software, and Pfizer Central Research, Sandwich, Kent, England, for the inhibitor samples and assistance they provided. We also thank Michael Bass for a molecular dynamics simulation of substrate-free P-450$_{CAM}$, modeled with Tyr96 and Phe193 side chains in an "up" conformation, which, despite the lack of a conformational switch in Tyr96 or Phe193, suggested that other aromatic groups near the putative access channel may be involved in substrate recognition and entry.

REFERENCES

Anders, M. W., Ed. (1985) *Bioactivation of Foreign Compounds*, Academic Press, Inc., New York.

Atkins, W. M., & Sligar, S. G. (1988) *J. Biol. Chem. 263*, 18842–18849.

Bernstein, F. C., Koetzle, T. F., Williams, G. J. B., Meyer, E. F., Jr., Brice, M. D., Rogers, J. R., Kennard, O., Shimanouchi, T., & Tasumi, M. (1977) *J. Mol. Biol. 112*, 535–542.

Debrunner, P. G., Gunsalus, I. C., Sligar, S. G., & Wagner, G. C. (1978) in *Metals in Biological Systems* (Sigel, H., Ed.) Vol. 7, pp 241–275, Marcel Dekker, New York.

Dorfman, L. M., & Adams, G. E. (1973) *Reactivity of the Hydroxyl Radical in Aqueous Solutions*, National Standard Reference Data System, National Bureau of Standards Publication, U.S. Department of Commerce, Washington, DC.

Gunsalus, I. C., & Sligar, S. G. (1978) *Adv. Enzymol. Relat. Areas Mol. Biol. 47*, 1–44.

Gunsalus, I. C., Meeks, J. R., Lipscomb, J. D., Debrunner, P. G., & Münck, E. (1974) in *Molecular Mechanisms of Oxygen Activation* (Hayaishi, O., Ed.) pp 559–613, Academic Press, New York.

Hendrickson, W. A., & Konnert, J. H. (1980) in *Computing in Crystallography* (Diamond, R., Ramaseshan, S., & Venkatesan, K., Eds.) pp 1301–1323, Indian Institute of Science, Bangalore, India.

Howard, A. J., Gilliland, G. L., Finzel, B. C., Poulos, T. L., Ohlendorf, D. H., & Salemme, F. R. (1987) *J. Appl. Crystallogr. 20*, 383–387.

Jones, T. A. (1978) *J. Appl. Crystallogr. 11*, 268–272.

Mázor, L. (1975) *Analytical Chemistry of Organic Halogen Compounds*, Pergamon Press, New York.

Nebert, D. W., & Gonzalez, F. J. (1987) *Annu. Rev. Biochem. 56*, 945–993.

Nebert, D. W., Eisen, H. J., Negishi, M., Lang, M. A., Hjelmeland, L. M., & Okey, A. B. (1981) *Annu. Rev. Pharmacol. Toxicol. 21*, 431–462.

Patai, S., & Rappoport, Z., Eds. (1983) *The Chemistry of Functional Groups, Supplement D: The chemistry of halides, pseudo-halides and azides*, John Wiley & Sons, New York.

Poulos, T. L., & Howard, A. J. (1987) *Biochemistry 26*, 8165–8174.

Poulos, T. L., Perez, M., & Wagner, G. C. (1982) *J. Biol. Chem. 257*, 10427–10429.

Poulos, T. L., Finzel, B. C., Gunsalus, I. C., Wagner, G. C., & Kraut, J. (1985) *J. Biol. Chem. 260*, 16122–16130.

Poulos, T. L., Finzel, B. C., & Howard, A. J. (1986) *Biochemistry 25*, 5314–5322.

Poulos, T. L., Finzel, B. C., & Howard, A. J. (1987) *J. Mol. Biol. 195*, 687–700.

Raag, R., & Poulos, T. L. (1989a) *Biochemistry 28*, 917–922.

Raag, R., & Poulos, T. L. (1989b) *Biochemistry 28*, 7586–7592.

Raag, R., & Poulos, T. L. (1991) *Biochemistry 30*, 2674–2684.

Raag, R., & Poulos, T. L. (1992) in *Frontiers in Biotransformation* (Ruckpaul, K., & Rein, H., Eds.) Vol. 7, pp 1–43, Akademie-Verlag, Berlin.

Raag, R., Swanson, B. A., Poulos, T. L., & Ortiz de Montellano, P. R. (1990) *Biochemistry 29*, 8119–8126.

Raag, R., Martinis, S. A., Sligar, S. G., & Poulos, T. L. (1991) *Biochemistry 30*, 11420–11429.

Richardson, K., Cooper, K., Marriott, M. S., Tarbit, M. H., Troke, P. F., & Whittle, P. J. (1990) *Rev. Infect. Dis. 12* (Suppl. 3), S267–S271.

Ullrich, V. (1979) *Top. Curr. Chem. 83*, 67–104.

Unger, B. P., Gunsalus, I. C., & Sligar, S. G. (1986) *J. Biol. Chem. 261*, 1158–1163.

Wagner, G. C., & Gunsalus, I. C. (1982) in *The Biological Chemistry of Iron* (Dunford, H. B., Dolphin, D., Raymond, K., & Sieker, L., Eds.) pp 405–412, Riedel, Boston.